2004

Investigation of Liquid Flow in Microchannels

D. Liu

S V. Garimella
Purdue University, sureshg@purdue.edu

INVESTIGATION OF LIQUID FLOW IN MICROCHANNELS

Dong Liu and Suresh V. Garimella[‡]
Cooling Technologies Research Center
School of Mechanical Engineering, Purdue University
West Lafayette, Indiana 47907-2088

Abstract

Liquid flow in microchannels is investigated both experimentally and numerically in this work. The experiments are carried out in microchannels with hydraulic diameters from 244 to 974 μm at Reynolds numbers ranging from 230 to 6500. The pressure drop in these microchannels is measured *in situ*, and is also determined by correcting global measurements for inlet and exit losses. Onset of turbulence is verified by flow visualization. The experimental measurements of pressure drop are compared to numerical predictions. Results from this work show that conventional theory may be used to successfully predict the flow behavior in microchannels in the range of dimensions considered here.

[‡] Corresponding author: (765) 494-5621, sureshg@ecn.purdue.edu

Nomenclature

D_h	Hydraulic diameter, μm
f	Darcy friction factor
H	Microchannel height, μm
l	Characteristic size of eddies in turbulent flow, m
L	Microchannel length, mm
P	Pressure, Pa
Q	Volume flow rate, m^3/s
Re	Reynolds number
u	Characteristic velocity scale of eddies in turbulent flow, m/s
U	Average velocity in microchannel, m/s
W	Microchannel width, μm
x^+	Entrance length, mm

Greek Symbols

α	Aspect ratio, H/W
δ	Uncertainty
ε	Dissipation rate, m^2/s^3
η	Kolmogorov length scale, m
μ	Fluid viscosity, $N \cdot s/m^2$
ν	Kinematic viscosity, m^2/s
ρ	Fluid density, kg/m^3
ΔP	Pressure difference, Pa

Subscripts

app	Apparent
fd	Fully developed conditions

Introduction

A number of investigations have been undertaken in the recent past to understand the fundamentals of fluid flow in microchannels, as well as to compare the heat transfer characteristics to those in conventional channels. This work has been driven in large part by the very high heat transfer rates that can be achieved with microchannel heat sinks for electronics cooling and other applications. However, published results have often been inconsistent, with wide discrepancies between different studies. For example, the friction factors have either been higher or lower than values predicted by classical laminar theory for conventional-sized ("macro") channels.[1,2] Another discrepancy concerns early transition from laminar to turbulent flow.[1,3] Possible reasons advanced to account for the deviation from classical theory include surface roughness effects,[3] electrical double layer effects,[4] and aspect ratio effects.[5] The capability of Navier-Stokes equations to adequately represent the flow and heat transfer behavior in microchannels has been called into question by these studies.

Recent reviews of the state of the art [6, 7] indicate that before predictions of flow and heat transfer rates in microchannels can be made with confidence, carefully designed experiments are needed to resolve the discrepancies in the literature and to provide practical information on the design of microchannel heat sinks.

In the present work, an experimental facility has been designed and fabricated to enable a careful investigation of single-phase liquid flow in microchannels with hydraulic diameters ranging from approximately 250 to 1000 μm. The Reynolds number of the flow was varied from 230 to 6500. The aims of this work are first to examine the validity of conventional theory in predicting the flow behavior in microchannels, and then to verify the Reynolds number range for transition from laminar to turbulent flow.

Experimental Apparatus

The experimental facility used for these experiments is shown schematically in Fig. 1. The facility consists of a liquid reservoir pressured by gas, microfilter, flowmeter, differential pressure transducer (diaphragm-type) with carrier demodulator, microchannel test section and computerized data acquisition system. A wide range of flow rates of deionized water from 0.08 to 1.06 liters/min can be achieved by varying the gas pressure. A turbine flowmeter with an infra-red flow sensor is used for measurement of flow rate. Optical access for flow visualization is available since the test section is made of plexiglass.

In the initial design, a variable-flow gear pump was used as the prime mover, but oscillations in the flow rate were observed. Since external perturbations could cause instability in the flow and interfere with flow transition, the test apparatus was revised for the flow to be driven by pressurized nitrogen gas. This approach was found to provide a smooth and steady flow, with pressures of up to 827 kPa (120 psi). By measuring the pressure drop along the microchannel and the flow rate through the microchannel, a friction factor is calculated.

Microchannel pressure measurements in the literature have been generally made between the inlet and exit of the test sections, beyond the actual length of the microchannels. Consequently, the measured pressure drops have inevitably included local losses due to the abrupt contraction at the inlet and the expansion at the outlet. It is crucial to appropriately account for these pressure losses in order to obtain sound results; the approach used for this correction has, however, not been clarified in sufficient detail in many published studies. To address this question further, two types of microchannel test sections were fabricated for the

present work as described in the following, to determine the methodology needed to achieve reliable pressure drop results.

A schematic representing the two different types of microchannel test sections is shown in Fig. 2. The microchannel test sections were fabricated from plexiglass, using a 3-axis CNC machine. The desired microchannel widths and aspect ratios were achieved by selecting high-speed steel jeweler's saws of different thickness and controlling the cutting depth. A list of the microchannel test sections investigated is provided in Table 1. The resulting surface roughness within the microchannels was measured with a profilometer and found to yield relative roughness (defined as the ratio of measured absolute roughness to the characteristic length, i.e. hydraulic diameter in the present study) of well below 3%. The effects of surface roughness are thus not likely to be critical in influencing the flow field.[8] The dimensions of the microchannel cross section were also carefully measured with an optical microscope, minimizing the uncertainty in determining hydraulic diameters D_h.

The two types of microchannel test sections studied differ in two respects: the microchannel length, and the position of pressure tap ports. For the first type, in which the microchannels are shorter (S-series), the pressure taps were placed in the inlet and outlet sections, as shown by the dashed lines in Fig. 2. For the second type, the channel length is longer (L-series) and the pressure taps were machined along the length of the microchannel itself, remote from the effects of the entrance and exit regions. A 100 μm-diameter microdrill was used for making the pressure taps. In this latter case, the measured pressure difference would be the actual pressure drop between the locations of the two pressure taps, with no additional considerations needed for losses. The pressure taps were carefully machined to avoid burs or other disturbances to the flow channel.

Data Reduction and Uncertainty Analysis

The experimental data in the present work were analyzed in the framework of conventional theory. The pressure drop and flow rate were measured to obtain the two most often used nondimensional parameters, the Reynolds number *Re* and the Darcy friction factor *f*:

$$\mathrm{Re} = \frac{\rho U D_h}{\mu} \tag{1}$$

$$f = \frac{\left(\Delta P / L\right) D_h}{\left(1/2\right) \rho U^2} \tag{2}$$

The experimental measurements were compared to predictions from conventional theory. For fully developed laminar flow in rectangular channels of channel aspect ratio α, the following expression from the literature[9] was used to predict the friction constant:

$$f\,\mathrm{Re} = 96\left(1 - 1.3553/\alpha + 1.9467/\alpha^2 - 1.7012/\alpha^3 + 0.9564/\alpha^4 - 0.2537/\alpha^5\right) \tag{3}$$

For fully developed turbulent flow, predictions were obtained following the Blasius solution:

$$f = 0.316/\mathrm{Re}^{0.25} \qquad (Re < 20{,}000) \tag{4}$$

In most practical applications, the microchannel is not long enough for the flow to become fully developed under laminar flow conditions. In such cases, the following expression for apparent friction factor accounts for both the developing and fully developed laminar flow regions in the channel [9]:

$$f_{app}\,\mathrm{Re} = \left[\left\{\frac{3.2}{(x^+)^{0.57}}\right\}^2 + (f\,\mathrm{Re})_{fd}^{\,2}\right]^{1/2} \tag{5}$$

where $(f\,\mathrm{Re})_{fd}$ is calculated as in eq. (3), and the entrance length x^+ is defined as

$$x^+ = L/\left(D_h \cdot \mathrm{Re}\right)$$

Similarly well-established correlations are, however, unavailable for turbulent developing flows.

Modifications must be made when calculating pressure drops for the short microchannels to exclude the pressure losses resulting from the inlet contraction and outlet expansion. The correction methodology used in this work is discussed in the Appendix. The pressure drop to be used in eq. (2) for the short microchannels is then:

$$\Delta P = (\Delta P)_{measured} - (\Delta P)_{loss} \tag{6}$$

The experimental uncertainties in the measurements were estimated using[10]:

$$\frac{\delta \mathrm{Re}}{\mathrm{Re}} = \left[\left(\frac{\delta Q}{Q} \right)^2 + \left(\frac{\delta H}{H} \right)^2 + \left(\frac{\delta W}{W} \right)^2 \right]^{1/2} \tag{7}$$

$$\frac{\delta f}{f} = \left[\left(\frac{\delta P}{P} \right)^2 + \left(\frac{\delta L}{L} \right)^2 + \left(\frac{\delta Q}{Q} \right)^2 + \left(3\frac{\delta H}{H} \right)^2 + \left(3\frac{\delta W}{W} \right)^2 \right]^{1/2} \tag{8}$$

The uncertainties in the terms above are estimated from manufacturers' specifications and dimensional measurement uncertainties as follows: δQ is ±1.01% of flowmeter reading; δL, δH and δW are 1 mm, 40 μm and 5 μm, respectively; δP is ±0.25% of pressure transducer full scale (138 kPa) including effects of linearity, hysteresis and repeatability. For a typical measurement (*e.g.*, case L2: L = 41 mm, H = 942 μm, W = 323 μm), the pressure drop varies from 4.8 to 77.9 kPa as the Reynolds number is increased from 379 to 3619, and the estimated uncertainties are:

$$\frac{\delta \mathrm{Re}}{\mathrm{Re}} = 4.6\%$$

$$5.3\% \le \frac{\delta f}{f} \le 8.9\%$$

For all the cases considered in this study, the uncertainties can be computed in the same manner as described by eqs. (7) and (8). For the long microchannels, the uncertainties ranged from 4.6 to 10.5% for Re and 5.3 to 11.8% for f. Similarly, for the short channels, the

corresponding uncertainties ranged from 4.9 to 9.5% for Re, and 6.2 to 10.9% for f. As indicated by eqs. (7) and (8), errors in measurement of the microchannel geometry are the greatest contributors to the uncertainty in friction factor. This uncertainty may be one source of discrepancies in the measurements reported in the literature.

Experimental Results and Discussion

Friction Factors

Experimental results for the long (L-series) microchannels are shown in Figs. 3 (a) to (d). The Darcy friction factor is plotted as a function of Reynolds number. Since the pressure drop in this case does not involve any inlet and exit losses, potential errors in correcting the measurements for losses are avoided. It is seen from Fig. 3 that for all the cases considered ($324 \leq D_h \leq 974$ μm), the experimental results agree closely with the theoretical predictions in the laminar region. At Re ≈ 2000, the friction factors from the experiments start to deviate from the laminar predictions, indicating the onset of transition. The onset of transition for the microchannels considered is thus seen to agree with the behavior in conventional channels.

Onset of Transition

Transition to turbulence arises essentially from the sensitivity of the flow field to perturbations such as small changes in initial conditions, boundary conditions, etc. In real flows, no strict theoretical limit exists for the critical Reynolds number at which transition will occur. According to linear instability analysis[11], the critical Reynolds number for a channel with aspect ratio $\alpha = 8$ should be higher than 10261, and will increase with decreasing aspect ratio. Experimental observations have shown that channel flow can stay laminar for Reynolds numbers

up to 50000 if completely undisturbed. With the presence of perturbations, the onset of turbulence will occur for a Re of 1800[12], below which the flow will remain laminar even with very strong disturbances.

Arguments have been extended in the literature that early transition occurs in microchannels at Reynolds numbers as low as 500.[3, 4] But recent studies have attributed these low transitional Reynolds numbers to possible experimental errors.[13] Other recent studies have indicated higher transitional Reynolds numbers of approximately 1500,[12, 14] which is closer to that observed in conventional channels. Results from the present work also suggest that no such early transition occurs, at least down to hydraulic diameters of approximately 200 μm. Figure 3 also indicates that the transition range extends up to Re = 4000 (Fig. 3b and 3c), and there are indications from Fig. 3(a) that the flow becomes fully turbulent at Re = 5000. These values compare favorably to Re = 3000 which is considered to be the minimum Reynolds number for fully turbulent flow[15] in conventional channels.

In turbulent flows, Kolmogorov microscales are the smallest scales representing the finest structure in the flow (the smallest feature size at which the kinetic energy is dissipated via viscosity, i.e. the smallest eddy). They are related to the rate of dissipation ε due to the fluctuating velocity components and the kinematic viscosity[16] ν

$$\eta = \left(\frac{\nu^3}{\varepsilon}\right)^{\frac{1}{4}} \tag{9}$$

$$\varepsilon = \frac{\left[u(l)\right]^3}{l} \tag{10}$$

It is expected that the smaller the Kolmogorov scales are, the more effective the kinetic energy dissipation via molecular viscosity, and the more turbulent the flow. In the "energy cascade"

concept,[17] the rate of energy transfer from large scales determines the dissipation rate ε that is at the end of the cascade. Therefore, the Kolmogorov scales can be calculated with information from the mean flow field, where the large eddies occur. Since any fine structure in the flow would be restricted by the physical dimension of the flow, if the characteristic length scale of the flow were smaller than the Kolmogorov length scale, the flow field would be dominated by viscous stresses and turbulence would not be sustained.

Taking $u(l)$ as the velocity fluctuation in the mean velocity field, which occurs over the microchannel characteristic dimension l (D_h in this case), the corresponding Kolmogorov length scales for water at 295 K in microchannels of various dimensions are estimated in Table 2.

Several observations can be made from the estimates in Table 2: (1) For fixed microchannel size, reduced fluctuations in the mean velocity field will result in a larger Kolmogorov length scale, as well as smaller dissipation rate. So the flow would tend to be more stable. (2) For fixed velocity fluctuations, decreasing the microchannel dimension will result in a larger value of η/l since $\eta/l \propto l^{-3/4}$. When this ratio exceeds unity, turbulent structures may not be sustained in the small physical dimensions available, thus preventing the flow from becoming fully turbulent. (3) For fixed velocity fluctuations, the impact of microchannel size on the turbulent flow becomes pronounced only when the channel size is sufficiently small. For instance, when $u(l) = 1$ m/s, l needs to be on the order of 1 mm before $\eta/l \approx 1$. The effect becomes less pronounced for larger dimensions, but is more apparent for reduced dimensions. This may help explain the trends in Fig. 3 – since all the microchannel hydraulic diameters considered are less than 1 mm, even for an aggressive estimate for velocity fluctuation $u(l)$ of 1 m/s, the Kolmogorov length scale will be larger than the microchannel dimension (D_h) which makes fully turbulent flow less likely. As a result, the experimental data fail to match the

theoretical predictions in the Reynolds number range of 3000 ~ 4000, which assume fully developed turbulence. (4) For a microchannel of 0.1 mm dimension, only when *u(l)* reaches 10 m/s is the Kolmogorov length scale small enough to become comparable to the microchannel dimension at which fully developed turbulent flow can be sustained. This implies that, for very small microchannel dimensions, it is very difficult to sustain fully developed turbulent flows. (5) The information on velocity fluctuations is crucial in the above estimates. This suggests the need for obtaining more detailed information in future research into turbulent microchannel transport.

Friction Factors with Pressure Losses

Experiments were also performed in short (S-series) microchannels to examine the validity of correcting for inlet and exit losses using conventional correlations (as described in the Appendix). Results for these short microchannels are shown in Figs. 4 (a) to (e). The symbols in the figures indicate measured pressure drops which have been corrected as per eq. (6). The good agreement between experiment and conventional correlations in the laminar regime validates the methodology for correction of inlet and exit losses. In the turbulent regime, on the other hand, satisfactory correlations for the losses are not readily available.

Flow Visualization

To verify the onset of transition to turbulence, flow visualization was performed using a dye entrained into the flow upstream of the microchannels. The pressure port was used as the dye-well from which a steady stream of potassium permanganate solution was released into the flow. Since the dye is a dilute aqueous solution, it can be considered to be neutrally buoyant.

The images were collected using a color video system consisting of a 6x-300x video inspection microscope and a CCD camera. The observations were made near the midpoint along the length of the microchannel.

In the flow visualization, onset of transition is considered to occur when the dye streaks entrained into the flow start to diffuse and blur. The measured flow rate allows a determination of the corresponding Reynolds number. Results for flow visualization in microchannels with hydraulic diameters of 271 and 470 μm are shown in Figs. 5 and 6. The flow is from left to right.

Figure 5 illustrates the flow behavior at different Reynolds numbers in the microchannel S2 (D_h = 271 μm). At low Reynolds numbers (Re = 761, 1230), there is virtually no diffusion of the dye streaks all along the channel, and the streakline remains clearly demarcated. At Re = 1942, although the dye streak is less distinct, this is a result of reduced dye density caused by the higher flow velocity, and not due to turbulent diffusion. Even at Re = 2216, the dye streaks can still be recognized, suggesting that the flow remains laminar in this entire Re range, as suggested also by the results in Fig. 4 (b).

Flow visualization results for a larger microchannel (S5, W = 480 μm) are shown in Fig. 6. The reduced liquid velocity for a given Reynolds number in this case, coupled with a larger field of view allows a better resolution. At low Reynolds numbers (Re = 588, 1078), there is no diffusion of the dye streaks all along the microchannel, and the straight streakline has sharp edges. At Re = 1802, the edge of the dye streak starts to blur, indicating the onset of transition. By Re = 2202, the dye is almost completely diffused. Transition to turbulence in this case may be considered to have occurred at a Reynolds number of approximately 1800. These

visualizations again agree with the observations from the measured pressure drops, which showed that the flow can stay laminar up to Re ≈ 2000.

Numerical Analysis

Computations of microchannel flow and heat transfer which include a consideration of the inlet/outlet sections are needed for any realistic microchannel heat sink implementation. The present simulations were targeted at evaluating the overall pressure drop in such a simulation.

A general-purpose finite-volume based CFD software package (FLUENT [18]) was used for these computations. The working fluid, which is water in this case, was considered to be incompressible, and its properties assumed constant. Only flow rates in the laminar regime were considered. The calculation domain is shown in Fig. 7. Results for simulations in the microchannel test section S5 (W = 480 μm, H = 460 μm) are presented here. The grid consists of 270,000 computational cells. A mesh of hexahedral elements was employed with the Cooper scheme.

To accurately resolve the flow field in critical regions such as within the microchannels and at the inlet/outlet interfaces, the mesh was locally refined. The inlet velocity was specified and an "outflow" condition assigned at the outlet. The convective terms were discretized using a first order upwind scheme for all equations. A computational grid of 15 × 15 × 60 cells was used within the microchannel. Simulations with different grids showed a satisfactory grid-independence for the results obtained with this mesh. For the case of Re = 1113, for instance, with the same inlet conditions the pressure drop along the microchannel was 7.83 kPa for the 15 × 15 × 60 mesh in the microchannel, and 7.99 kPa for a coarser mesh (10 × 10 × 50).

The liquid is driven through the inlet and is accelerated at the abrupt contraction into the microchannels. Either the pressure drop within the microchannel or the entrance loss dominates the overall pressure drop, depending on the flow rate. This trend is clearly indicated in Fig. 8, which shows that the pressure drop increases significantly at the higher flow rates. A closer examination of the results in Fig. 8 reveals several interesting features: (1) The significant flow contraction at the entrance to the microchannel causes a sharp drop in the pressure. (2) It is clear that the inlet pressure losses account for quite a large fraction of the overall pressure drop at the higher flow rates, pointing to the importance of a careful consideration of these losses in microchannel heat sink design. (3) The length required for the pressure drop per unit length to reach a constant value may be determined as

$$x / D_h = C\,\mathrm{Re} \tag{11}$$

where C is a constant depending on the geometry, (0.033, 0.046 and 0.057 for aspect ratios of 10, 5 and 1, respectively [19]). It can be seen in Fig. 9 that, at low Reynolds numbers, the flow becomes fully developed some distance into the microchannel; *e.g.*, at Re = 511, the pressure gradient is nearly constant from x = 0.055 m, signifying an entrance length of 0.012 m (this compares to a value of x predicted from eq. (11) of 0.011 m). In contrast, at higher Re, the flow continues to develop throughout the length of the microchannel; *e.g.*, at Re = 1113, the entrance length is 0.024 m which covers virtually the entire length of the microchannel (L = 0.025 m). Consequently, the apparent friction factor, as in eq. (5), should be employed in interpreting the experimental data in such developing flow in microchannels.

A comparison of the numerically predicted overall pressure drop in the microchannels against the experimentally determined values is shown in Table 3. The two sets of results are seen to show satisfactory agreement, considering the complexity of the system-level flow field,

which suggests that a conventional CFD analysis approach can be employed in predicting flow behavior in the microchannels considered in this study.

Conclusions

Experimental measurements and numerical simulations have been performed, along with flow visualization and analysis, to study the behavior of liquid flow in microchannels. It is found that conventional theory offers reliable predictions for the flow characteristics in microchannels up to a Reynolds number of approximately 2000, in the range of hydraulic diameters considered (244 to 974 μm). There is also support for the argument that the development of fully turbulent flow is retarded in microchannels. The estimated Kolmogorov length scales suggest that the reduced microchannel size may have a significant impact on the development of turbulence. The onset of transition to turbulence in microchannels was qualitatively corroborated by flow visualization. The fact that the results of numerical simulations were in satisfactory agreement with the experimental measurements indicates that commercial software packages can be employed to aid the study of flow characteristics in microchannels.

Support for this work provided by NSF and industry members of the Cooling Technologies Research Center (http://widget.ecn.purdu.edu/~CTRC), an NSF Industry/University Cooperative Research Center at Purdue University, is gratefully acknowledged.

Appendix: Pressure Loss Correction

The construction of a microchannel heat sink usually involves contraction and expansion at the entrance and exit of the microchannels. These abrupt flow area changes introduce

additional local pressure drops. The overall pressure loss through the microchannel system consists of three parts[20]:

$$\Delta P = (P_1 - P_2) + (P_2 - P_3) + (P_3 - P_4) \qquad \text{(A1)}$$

in which $(P_2 - P_3)$ is the pressure drop in the microchannel, $(P_1 - P_2)$ is the contraction pressure loss, and $(P_3 - P_4)$ is the expansion pressure loss. Figure A1 illustrates the locations of pressures 1, 2, 3 and 4.

The pressure loss due to flow contraction at the entrance is given by:

$$P_1 - P_2 = (1 - (\frac{A_2}{A_1})^2 + K_1)\frac{1}{2}\rho U_2{}^2 + \frac{f_1 L_1}{D_1}\frac{1}{2}\rho U_1{}^2 \qquad \text{(A2)}$$

where A_1 is the inlet cross sectional area, and $A_2 = \sum_i A_{2i}$ = sum of flow areas. For laminar flow, the non-recoverable loss coefficient is given by

$$K_1 = 0.0088\ \alpha^2 - 0.1785\ \alpha + 1.6027 \qquad \text{(A3)}$$

Since the inlet section is usually too short for the flow to become fully developed, *fRe* should be evaluated from eq. (5). For turbulent flow, the non-recoverable loss coefficient is given by

$$K_1 = \frac{1}{2}(1 - \frac{A_2}{A_1}) \qquad \text{(A4)}$$

The pressure loss due to flow expansion at the exit has to be considered separately for laminar and turbulent flows because of the non-uniform flow profile at the exit. For laminar flow, the exit pressure loss is given by

$$\frac{P_3 - P_4}{\frac{1}{2}\rho U_2{}^2} = -2\beta\frac{A_2}{A_3}(1 - \frac{A_2}{A_3}) + \frac{f_3 L_3}{D_3} \qquad \text{(A5)}$$

where A_3 is the outlet cross sectional area, and $A_2 = \sum_i A_{2i}$ = sum of flow areas, and the flow profile factor $\beta = 1.33$. For turbulent flow, the pressure loss is estimated by

$$\frac{P_3 - P_4}{\frac{1}{2}\rho U_2^{\,2}} = (\frac{A_2}{A_3})^2 - 1 + K_3 + \frac{f_3 L_3}{D_3} \qquad \text{(A6)}$$

where the non-recoverable loss coefficient is

$$K_3 = (1 - \frac{A_2}{A_3})^2 \qquad \text{(A7)}$$

References

[1] Peng, X. F., Peterson, G. P., and Wang, B. X., "Frictional flow characteristics of water flowing through microchannels," *Experimental Heat Transfer*, Vol. 7, 1994, pp. 265-283.

[2] Yu, D., Warrington, R., Barron, R., and Ameel, T., "An experimental and theoretical investigation of fluid flow and heat transfer in microtubes," *ASME/JSME Thermal Engineering Conference*, Vol. 41, 1995, pp. 523-530.

[3] Mala, G. M. and Li, M., "Flow characteristics of water in microtubes," *Int. J. Heat and Fluid Flow*, Vol. 20, 1999, pp. 142-148.

[4] Mala, G. M., Li, D. and Dale, J. D., "Heat transfer and fluid flow in microchannels," *Int. J. Heat Mass Transfer*, Vol. 40, 1997, pp. 3079-3088.

[5] Papautsky, I., Gale, B. K., Mohanty, S., Ameel, T.A. and Frazier, A. B., "Effects of rectangular microchannel aspect ratio on laminar friction constant," 2000, (unpublished, from authors' website).

[6] Sobhan, C. B. and Garimella, S. V, "A comparative analysis of studies on heat transfer and fluid flow in microchannels," *Microscale Thermophysical Engineering*, Vol. 5, 2001, pp. 293-311.

[7]Garimella, S. V. and Sobhan, C. B., "Transport in microchannels – A critical review," *Annual Review of Heat Transfer*, Vol. 13, 2002.

[8] Xu, B., Ooi, K. T., Wong, N. T. and Choi, W.K., "Experimental investigation of flow friction for liquid flow in microchannels," *Int. Comm. Heat Mass Transfer*, Vol. 27, 2000, pp. 1165-1176.

[9] Shah, R. K. and London, A. L., " Laminar flow forced convection in ducts," *Advances in Heat Transfer*, Supplement 1, Academic Press, 1978.

[10] Figliola, R. S. and Beasley, D. E., *Theory and Design for Mechanical Measurements*, John Wiley, New York, 2000.

[11] Tatsumi, T. and Yoshimura T., "Stability of the laminar flow in a rectangular duct," *Journal of Fluid Mechanics*, Vol. 212, 1990, pp. 437-449.

[12] Sharp, K.V., Adrian, R. J. and Beebe, D. J., "Anomalous transition to turbulence in microtubes," MEMS-Vol. 2, ASME 2000, 2000, pp. 461-466.

[13] Obot, N. T., "Toward a better understanding of friction and heat/mass transfer in microchannels - A literature review," Heat *Transfer and Transport Phenomena in Microsystems*, Begell House, New York, pp.72-80, 2000.

[14] Harms, T. M., Kazmierczak, M. J. and Gerner, F. M., "Experimental investigation of heat transfer and pressure drop through deep microchannels in a (110) silicon substrate," *Procs. ASME Heat Transfer Division*, Vol. 1, 1997, pp. 347-357.

[15] Patel, V. C. and Head, M. R., "Some observations on skin friction and velocity profiles in fully developed pipe and channel flows," *Journal of Fluid Mechanics*, Vol. 38, 1969, pp. 181-201.

[16] Tennekes, H. and Lumley, J. I., *A First Course in Turbulence*, MIT Press, 1972.

[17] Pope, S. B., *Turbulent Flows*, Cambridge University Press, 2000.

[18] *Fluent User's Guide*, Fluent Inc., Lebanon, New Hampshire, 1998.

[19] Hartnett, J. P., Koh, J. C. Y. and McComas, S. T., "A comparison of predicted and measured friction factors for turbulent flow through rectangular ducts," *Journal of Heat Transfer*, Vol. 84, 1962, pp. 82 –88.

[20] R. D. Blevins, *Applied Fluid Dynamics Handbook*, Krieger Pub. Co., 1992, pp. 77-78.

FIGURE CAPTIONS

Figure 1. Schematic of the experimental apparatus.

Figure 2. Schematic of the microchannel test section (top cover not shown).

Figure 3. Friction factor variation with Reynolds number in long microchannels (laminar predictions from eq. 3, turbulent from eq. 4).

Figure 4. Corrected friction factor variation with Reynolds number in short microchannels (laminar predictions from eq. 5, turbulent from eq. 4).

Figure 5. Flow visualization in a short microchannel (S2: W = 180 μm, D_h = 271 μm).

Figure 6. Flow visualization in a wider microchannel(S5: W = 480 μm, D_h = 470 μm).

Figure 7. Computational domain for flow calculations in the microchannel test section.

Figure 8. Pressure drop for different Reynolds numbers (S5: D_h = 470 μm).

Figure 9. Pressure gradient in the microchannel for different Reynolds numbers (S5: D_h = 470 μm).

Figure A1. Top and side views of the microchannel test section (including inlet, microchannel and outlet sections; *D* denotes the corresponding hydraulic diameters, *L* the lengths, A the areas, and *U* the mean velocities. Position 1 and 4 are the locations of pressure taps).

Figure A2. Entrance contraction.

Figure A3. Exit expansion.

Table 1. Dimensions of the microchannels tested.

Test #	Number of Channels	W (μm)	H (μm)	L (mm)	D_h (μm)	α (H/W)
S1	5	170	433	25.4	244	2.55
S2	5	180	551	25.4	271	3.06
S3	5	285	731	25.4	410	2.56
S4	5	310	885	25.4	459	2.85
S5	5	480	460	25.4	470	0.96
L1	5	222	597	41.0	324	2.69
L2	3	323	942	41.0	481	2.92
L3	3	450	384	41.0	414	0.85
L4	3	1061	900	41.0	974	0.85

Table 2. Estimation of Kolmogorov length scale (kinematic viscosity $\nu = 0.00096\ m^2/s$).

Velocity fluctuation *u(l)* (m/s)	Channel size *l* (m)	Dissipation rate ε (m^2/s^3)	Kolmogorov length scale η (m)	η/l
1	0.1	10	0.0031	0.03
0.1	0.1	0.01	0.0172	0.17
1	0.01	1×10^2	0.00172	0.17
0.1	0.01	0.1	0.0097	0.97
1	0.001	1×10^3	0.00097	0.97
0.1	0.001	1	0.0055	5.50
1	0.0001	1×10^4	0.00055	5.50
0.1	0.0001	10	0.0031	31.00
10	0.0001	1×10^7	0.000097	0.97

Table 3. Measured and predicted overall pressure drops in the S5 microchannels.

Re	ΔP-numerical (Pa)	ΔP-exp. (Pa)	Difference
511	5012	5523	9%
602	6254	6765	8%
808	9119	9665	6%
960	11358	12288	8%
1113	13953	15463	10%
1357	18011	20158	11%
1761	29114	31203	9%
1960	33021	37279	11%

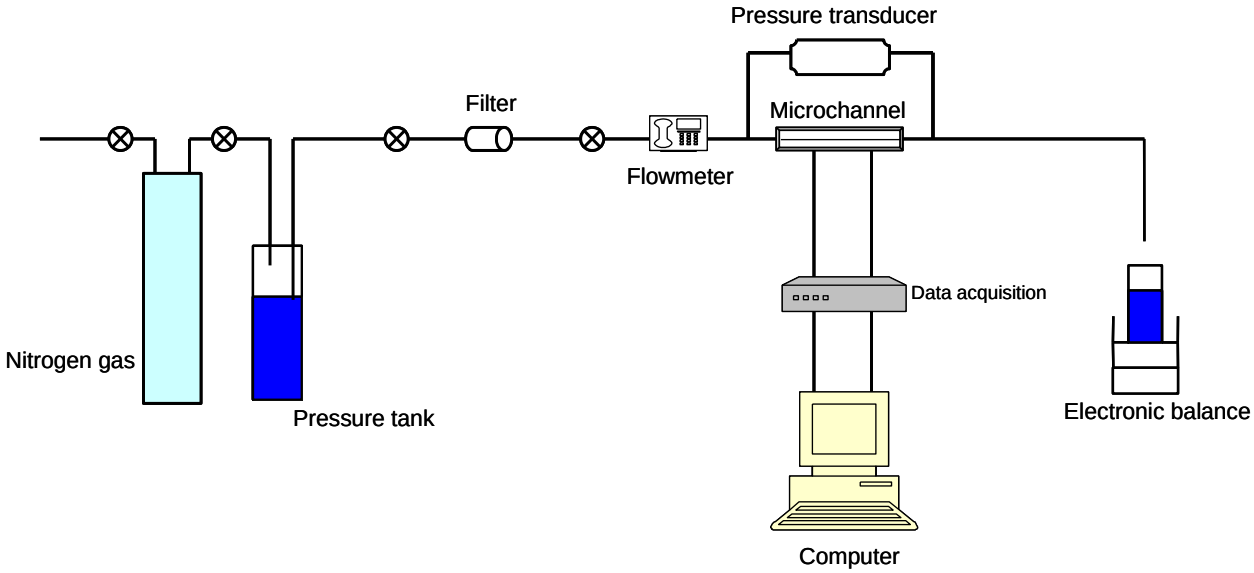

Figure 1. Schematic of the experimental apparatus.

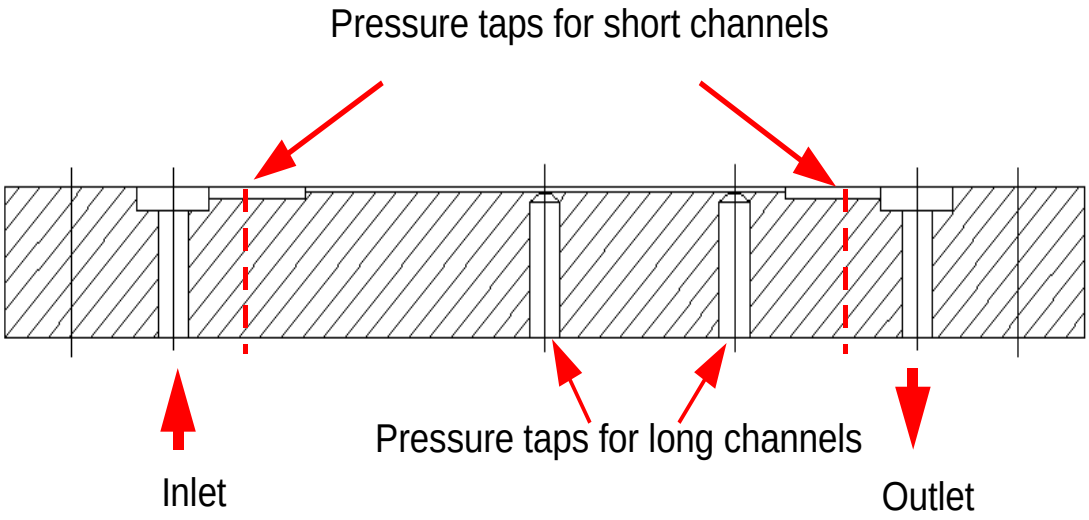

Figure 2. Schematic of the microchannel test section (top cover not shown).

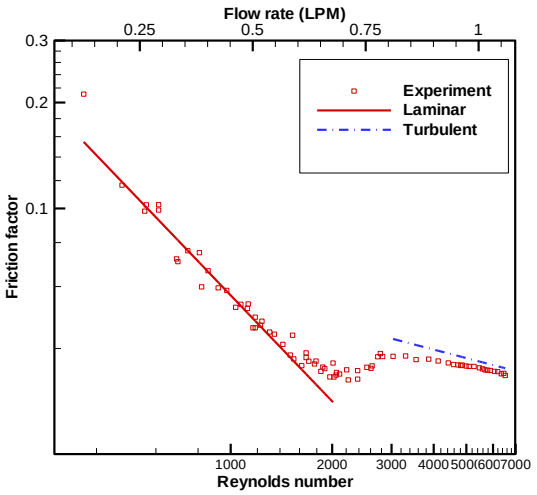

(a) L4 (D_h = 974 μm)

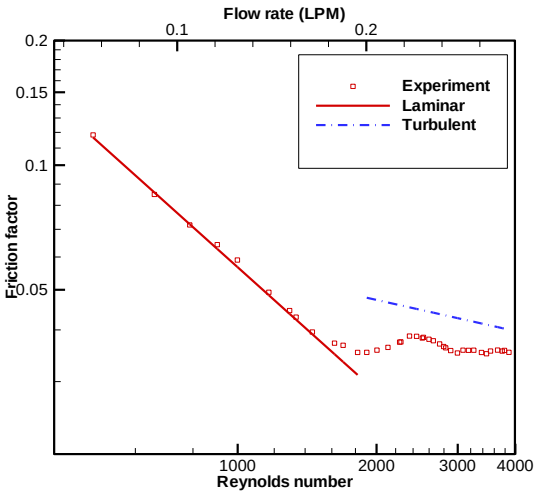

(b) L3 (D_h = 414 μm)

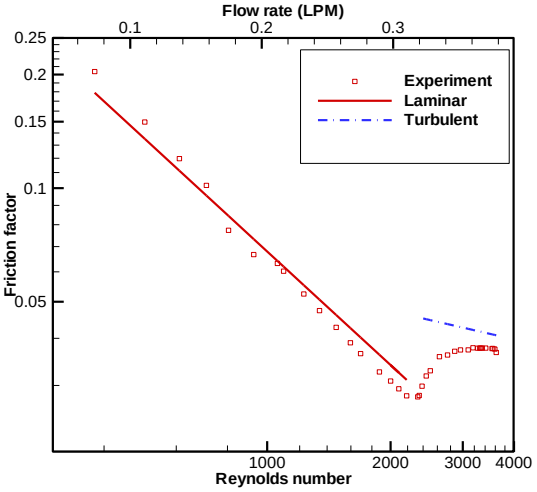

(c) L2 (D_h = 481 μm)

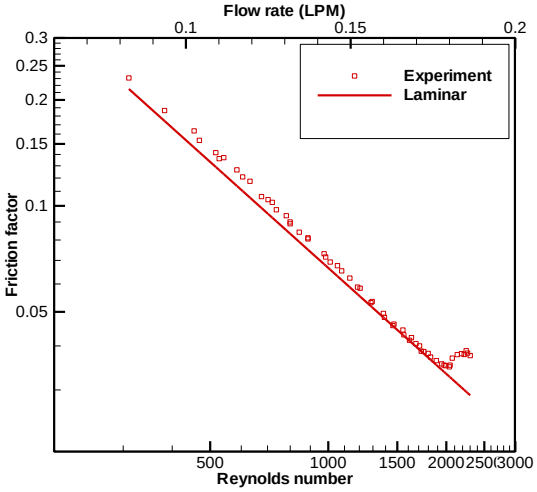

(d) L1 (D_h = 324 μm)

Figure 3. Friction factor variation with Reynolds number in long microchannels (laminar predictions from eq. 3, turbulent from eq. 4).

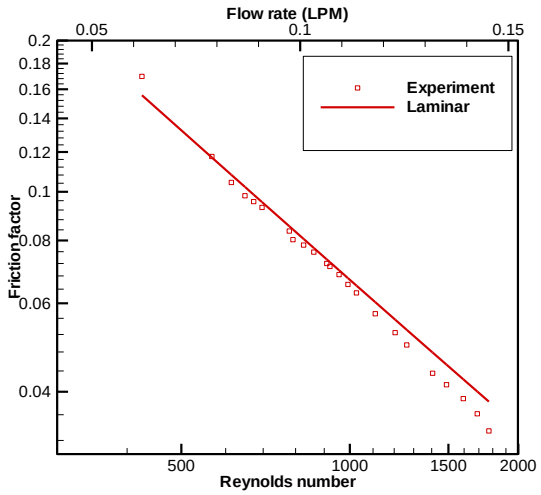

(a) S1 (D_h = 244 μm)

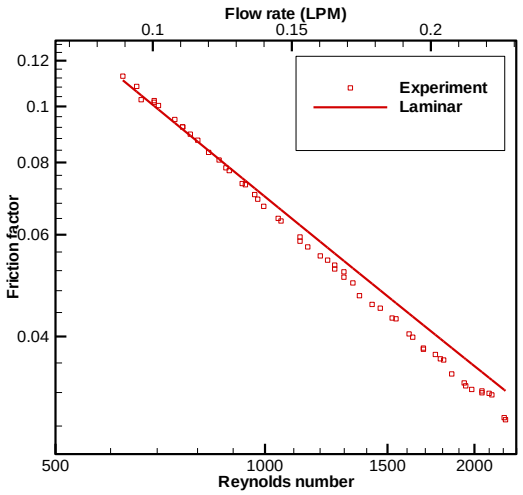

(b) S2 (D_h = 271 μm)

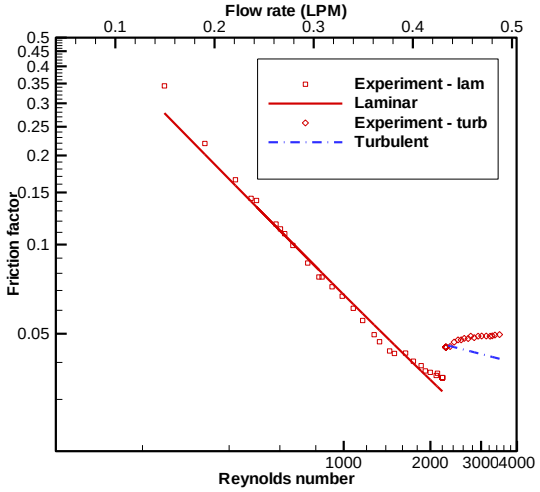

(c) S3 (D_h = 410 μm)

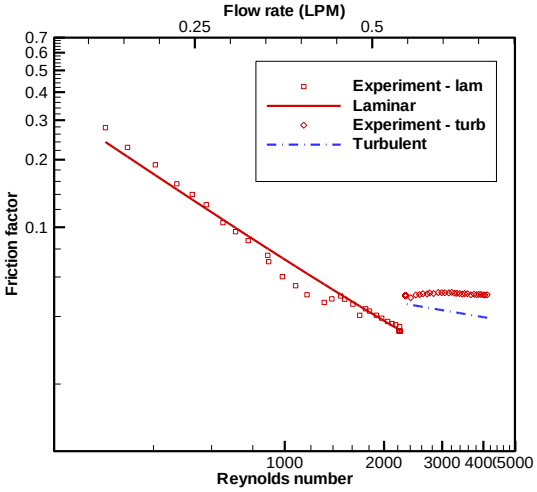

(d) S4 (D_h = 459 μm)

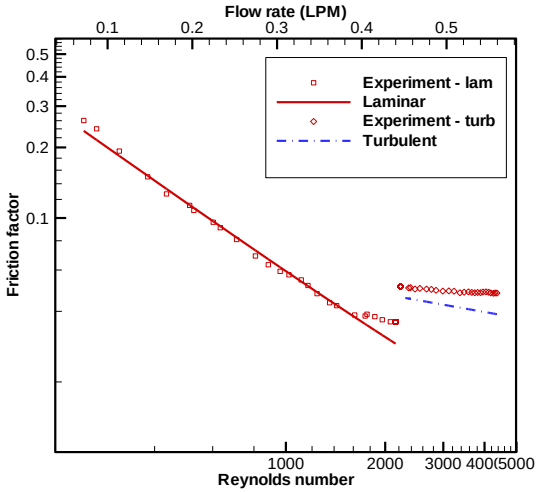

(e) S5 (D_h = 470 μm)

Figure 4. Corrected friction factor variation with Reynolds number in short microchannels (laminar predictions from eq. 5, turbulent from eq. 4).

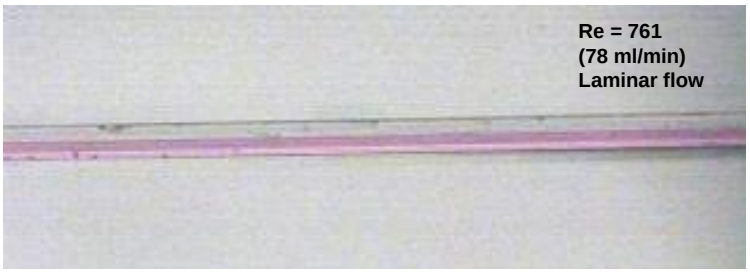

(a)

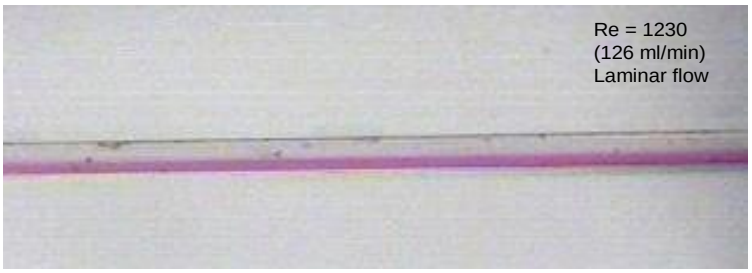

(b)

(c)

(d)

Figure 5. Flow visualization in a short microchannel (S2: W = 180 μm, D_h = 271 μm).

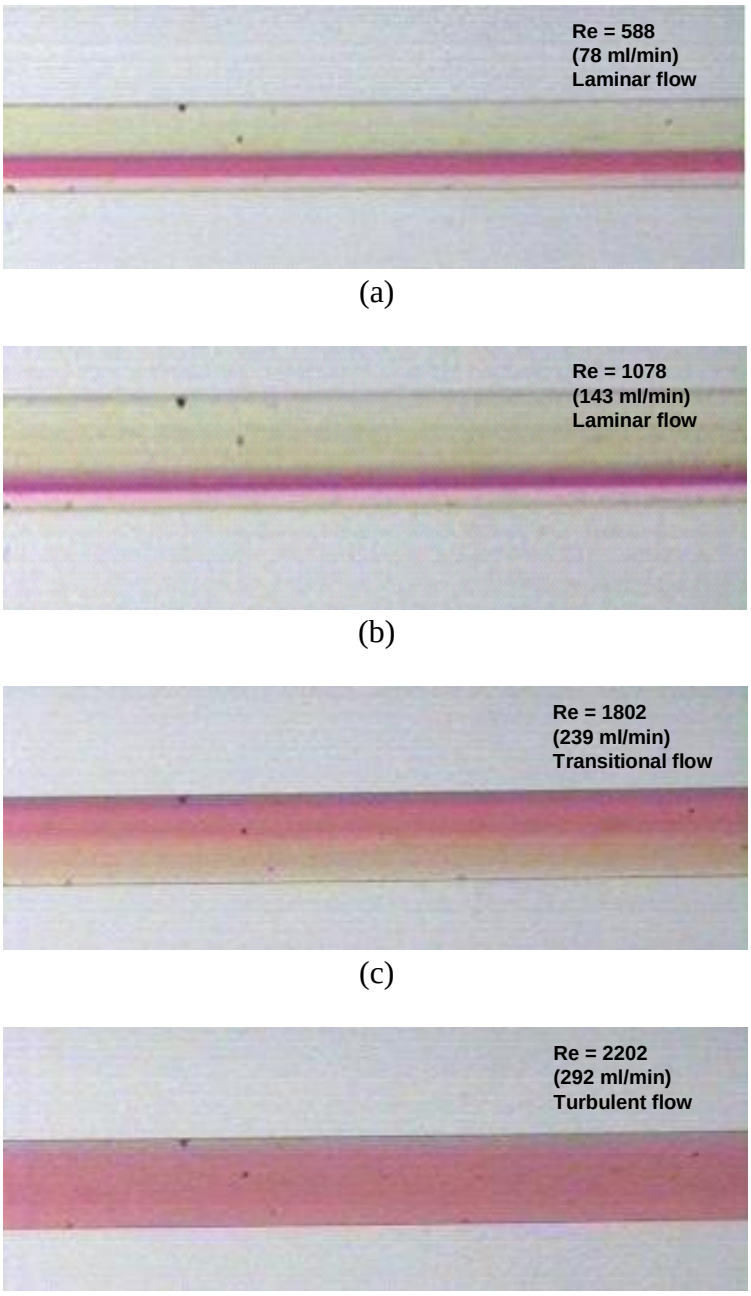

Figure 6. Flow visualization in a wider microchannel (S5: W = 480 μm, D_h = 470 μm).

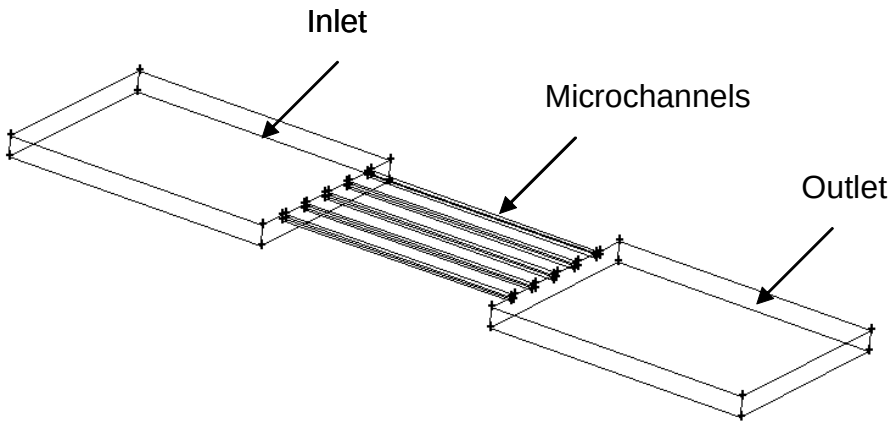

Figure 7. Computational domain for flow calculations in the microchannel test section.

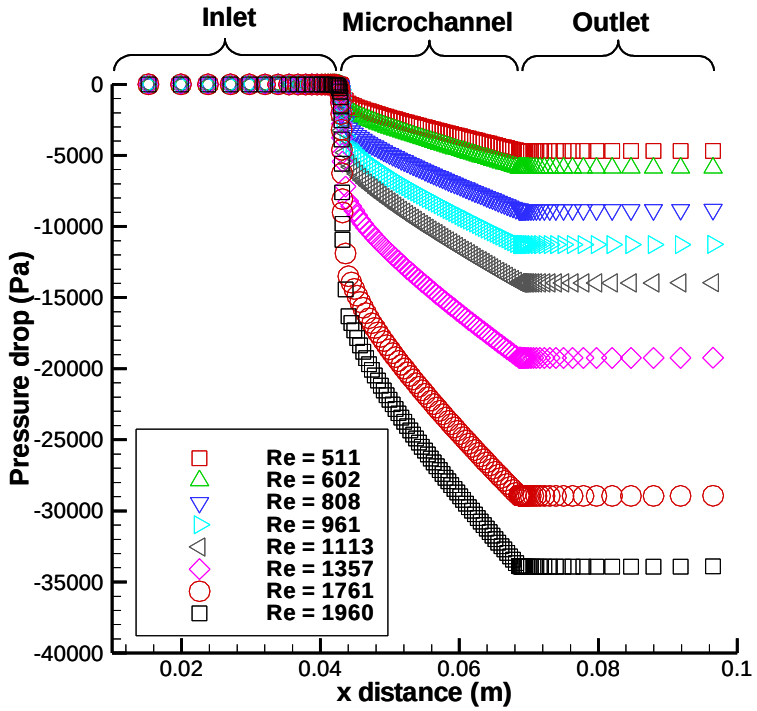

Figure 8. Pressure drop for different Reynolds numbers (S5: D_h = 470 μm).

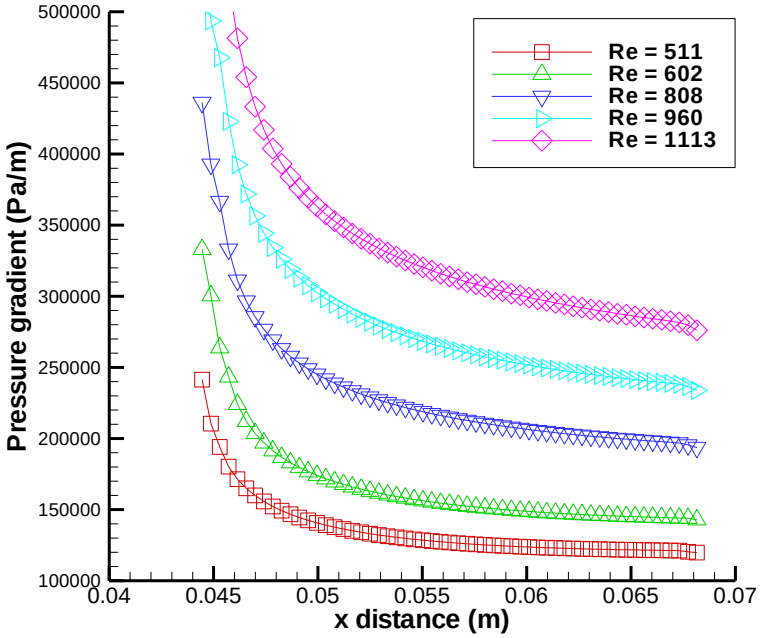

Figure 9. Pressure gradient in the microchannel for different Reynolds numbers (S5: D_h = 470 μm).

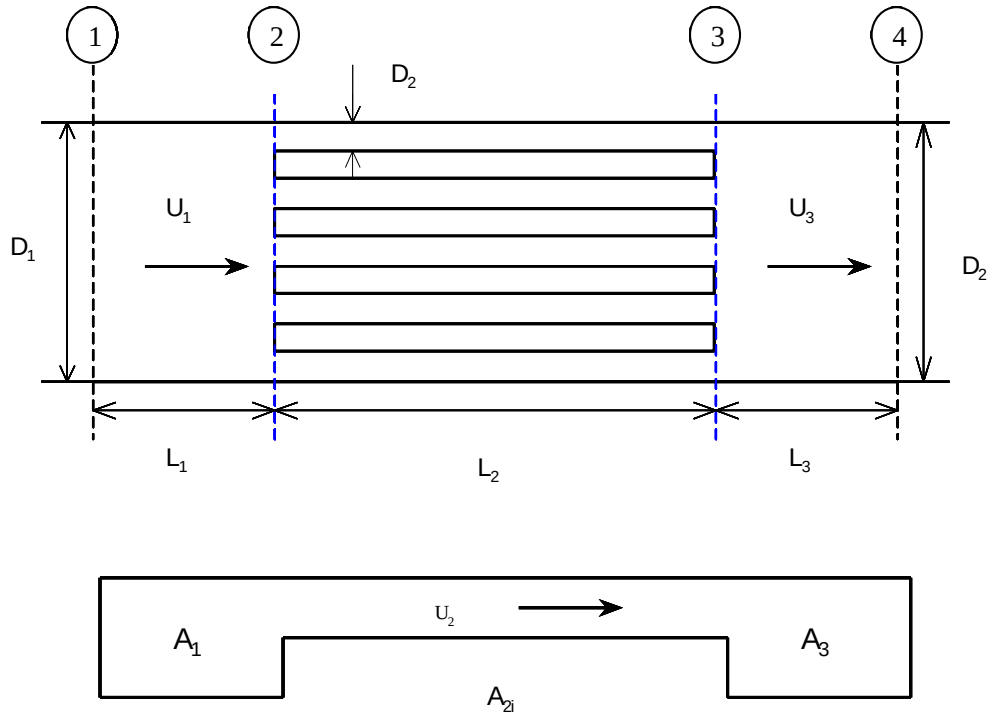

Figure A1. Top and side views of the microchannel test section including inlet, microchannel and outlet sections; *D* denotes the corresponding hydraulic diameters, *L* the lengths, A the areas, and *U* the mean velocities. Position 1 and 4 are the locations of pressure taps.

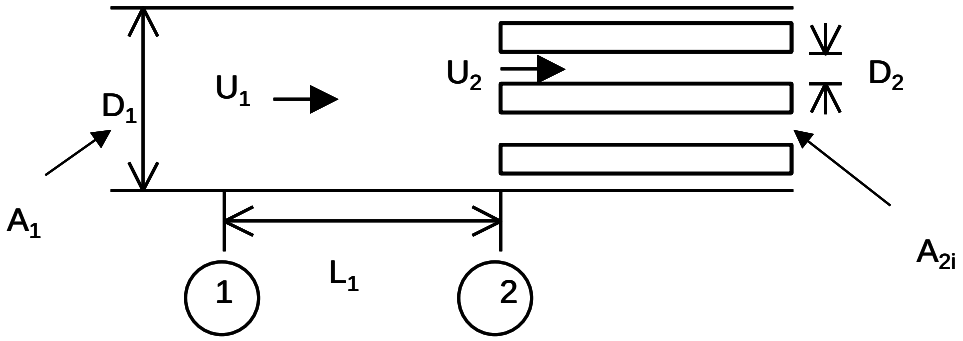

Figure A2. Entrance contraction.

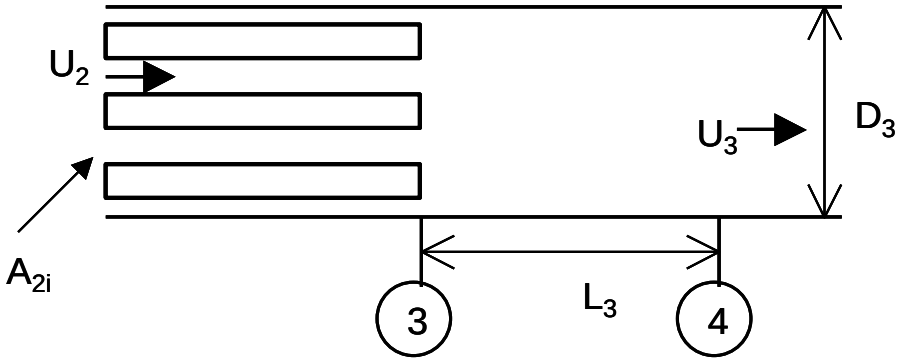

Figure A3. Exit expansion.